Diagonal and off-diagonal thermal conduction with resonant phonon scattering in Ni_3TeO_6

Heejun Yang [1], Xianghan Xu [2], Jun Han Lee [3], Yoon Seok Oh [3], Sang-Wook Cheong [2], and Je-Geun Park [1,4,*]

[1] *Department of Physics and Astronomy, Seoul National University, Seoul 08826, Republic of Korea*
[2] *Rutgers Center for Emergent Materials, and Department of Physics & Astronomy, Rutgers University, Piscataway, New Jersey 08854, USA*
[3] *Department of Physics, Ulsan National Institute of Science and Technology, Ulsan 44919, Republic of Korea*
[4] *Institute of Applied Physics, Seoul National University, Seoul 08826, Republic of Korea*

(Received 1 June 2022; revised 3 October 2022; accepted 5 October 2022; published 17 October 2022)

The coupling between phonon and magnon is ubiquitous in magnetic materials and plays a crucial role in many aspects of magnetic properties, most notably in spintronics. Yet, this academically and technologically interesting problem still poses a severe challenge to a general understanding of the issue in certain materials. We report that Ni_3TeO_6 exhibits clear evidence of significant magnon-phonon coupling in both longitudinal thermal conductivity (κ_{xx}) and thermal Hall coefficient (κ_{xy}). The Debye-Callaway model, a phenomenological description for phonon heat conduction, can explain the measured magnetic field dependence of $\kappa_{xx}(H)$: phonon scattering from spin fluctuation in the paramagnetic phase and additional scattering due to magnon-phonon coupling in the collinear antiferromagnetic phase. We further suggest that a similar approach could be applied to understand the finite κ_{xy} values in Ni_3TeO_6.

DOI: 10.1103/PhysRevB.106.144417

I. INTRODUCTION

Phonons are the dominant heat carrier and usually determine the overall thermal transport properties of most materials. The Debye-Callaway model [1], a standard phenomenological model, captures the essential temperature dependence. But there has been a long-standing question about how these phonons can interact with magnons, another fundamental quasiparticle in magnetic materials—this question goes back to the seminal paper by Kittel [2]. Despite the natural appeal of the idea, one had to wait for a considerable time before seeing actual experiments done with access to detailed precise measurements of both phonons and magnons [3,4].

These recent works primarily concern the case in which the bands of the magnon and phonon get coupled to each other. But there can be another case of magnon-phonon coupling, which is the resonant scattering of phonons via magnons [5–7]. The latter case is relatively rare because it requires the more stringent condition that magnons should have a large density of states at the right energy for the coupling to be realized. Recently, the magnon-phonon coupling has had renewed interest since the latest theoretical studies suggest that the magnon-phonon coupled term can produce nontrivial Berry curvature to its original Hamiltonian in several magnetic materials [8–11].

Observing Berry phase effects has been regarded as one piece of evidence for verifying the existence of novel quasiparticles [12,13], magnon topology [14–16], and topological phase transition [17] in magnetic insulators. For this reason, the thermal Hall effect, the thermal analog of the electric Hall effect, was proposed as one experimental method to detect such topological effects of the spin system directly. In principle, phonon can also possess Berry curvature with possible phonon Hall effect (PHE) [18,19], which implies a thermal Hall effect mainly governed by phonons. However, the typical size of the PHE was expected to be negligible compared to its magnetic origin, as in $Tb_3Ga_5O_{12}$ [20], the first material showing PHE. Indeed, several successful thermal Hall effect measurements from magnons [21–24], nontrivial spin excitation in a frustrated lattice [25–28], and Majorana fermions [29–31] were reported so far without considering the phonon contribution.

However, there has been a new twist in these thermal Hall effect studies with a series of unexpectedly significant PHE: multiferroicity [32], quantum paraelectricity [33], structural domain [34], and pseudogap phase in cuprate [35–37]. These latest results all seem to point towards possibly genuine phonon effects. One common feature of these systems is that the overall temperature dependence between longitudinal thermal conductivity (κ_{xx}) and thermal Hall coefficient (κ_{xy}) are quite similar to one another. With an apparently dominant phonon contribution to κ_{xx} for an insulating system, the similar temperature dependence between $\kappa_{xx}(T)$ and $\kappa_{xy}(T)$ can be interpreted as that $\kappa_{xx}(T)$ and $\kappa_{xy}(T)$ would share the same origin, a likely candidate being phonons [34–38]. Moreover, recent studies showed that such similar temperature dependence between $\kappa_{xx}(T)$ and $\kappa_{xy}(T)$ can also be found in other more exotic systems: e.g., the Kitaev quantum spin liquid candidate α-$RuCl_3$ [39] and kagome antiferromagnet Cd-kapellasite [40]. They suggested that sizable κ_{xy} values found in the experiments might not only be solely from Majorana fermions or other magnetic origin, but also from phonons [39–41]. Unfortunately, estimating the phonon contribution in κ_{xy} is still hard with little information on detailed mechanisms for PHE [18,19,42–44].

*jgpark10@snu.ac.kr

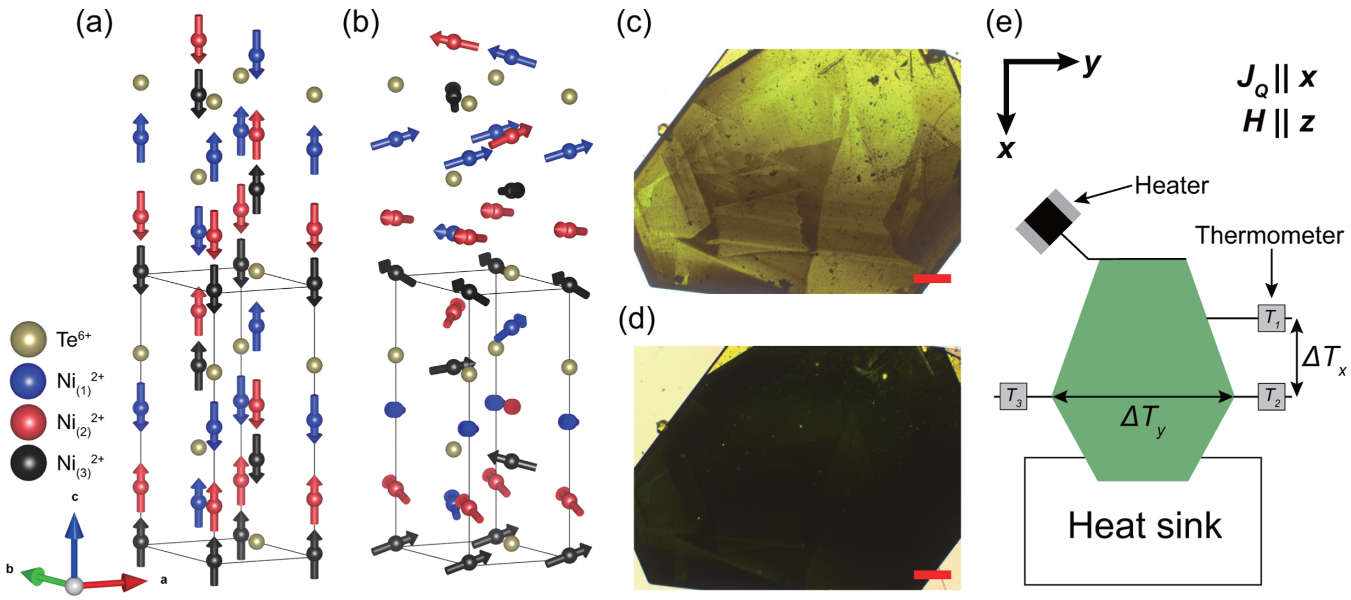

FIG. 1. Magnetic structure and photo of Ni_3TeO_6 sample and schematic of thermal transport experimental setup. (a) Collinear antiferromagnetic structure of the low-field phase. (b) The incommensurate conical spiral magnetic structure of the spin-flopped phase, as suggested in Ref. [49]. (c), (d) Images of Ni_3TeO_6 sample taken using a transmission polarized optical microscope. Scale bars are 200 μm. (c) The sample shows transparent green color with parallel polarizer and analyzer. (d) Slight rotation of the analyzer makes the chiral domain visible. The overall dark color indicates a single chiral domain in the sample. (e) Schematic of thermal transport experimental setup. Heat current (J_Q) and magnetic field (H) are applied along the *ab* plane and the *c* axis of the sample, respectively.

Ni_3TeO_6 (NTO) can be one good example of the PHE since the specific heat of NTO remains nearly constant with various magnetic fields applied along the crystallographic *c* axis [45], implying phonon dominant κ_{xx} in NTO [32]. It is also noteworthy that NTO is a polar magnet with other interesting properties: huge magnetoelectric effect [46] and clear phonon peak shift in infrared spectroscopy across the antiferromagnetic (AFM) phase transition [47], indicating significant spin-phonon coupling. All these suggest a possible PHE in NTO. There are also two distinct magnetic structures below the Néel temperature (T_N): a collinear AFM structure with an easy axis along the *c* axis [48] in the absence of the magnetic field [Fig. 1(a)] and an incommensurate conical spiral structure [49] of spin-flopped phase above the critical field ($\mu_0 H_c \sim 8.5$ T) applied along the *c* axis [46] [Fig. 1(b)]. We anticipate that this magnetic phase transition could affect both κ_{xx} and κ_{xy}, giving another clue for PHE.

In this paper, we report both in-plane κ_{xx} and κ_{xy} of NTO with the magnetic field applied along the *c* axis up to 14 T. $\kappa_{xx}(T)$ seems to follow the conventional behavior of phonon thermal conductivity with pronounced suppression around T_N due to paramagnetic spin fluctuations. Observed $\kappa_{xy}(T)$ is still finite up to high temperature, twice T_N, indicating that the PHE scenario is more appropriate than magnons. Moreover, the overall temperature dependence of $\kappa_{xy}(T)$ is similar to $\kappa_{xx}(T)$, further suggesting the PHE in NTO. On the other hand, $\kappa_{xx}(H)$ shows two opposite-field dependences between the paramagnetic and AFM phases: slight increasing $\kappa_{xx}(H)$ in $T > T_N$, and more complex decreasing $\kappa_{xx}(H)$ in $T < T_N$. We used the Debye-Callaway model including the resonant phonon scattering process [1,50–53] from magnons to find that it gives a fair phenomenological understanding of κ_{xx} for $T < T_N$ and $H < H_c$. We propose that such magnon-phonon interaction would also be a dominant factor for κ_{xy}.

II. EXPERIMENTAL METHODS

Ni_3TeO_6 single crystals were grown by a flux method modified from a previous report [54]. Stoichiometric Na_2CO_3 and TeO_2 powders were mixed and sintered at 850 °C for 10 h to make a Ni_3TeO_6 polycrystalline precursor. For single crystal growth, powders of Ni_3TeO_6:V_2O_5:TeO_2:NaCl:KCl = 1:1.5:3:3:1.5 in the molar ratio were mixed and filled into a platinum crucible. The crucible was kept at 850 °C for 10 h before being slowly cooled to 500 °C at a 2 °C/h rate, after which the heaters were switched off for natural cooling to room temperature. Ni_3TeO_6 crystals with a typical size of 1.5 mm × 1.5 mm × 0.1 mm were mechanically separated from the product after overnight bathing in hot 1 mole NaOH. The chirality of Ni_3TeO_6 crystals was determined by a polarized-light optical microscope [55]. Figures 1(c) and 1(d) show that the Ni_3TeO_6 sample used in this study consists of a single chiral domain.

DC magnetic susceptibility (χ_{dc}) was measured by a Quantum Design magnetic property measurement system. Thermal conductivity was measured using a homemade setup, which works based on a conventional steady-state method with one heater and three thermometers. To minimize errors from strong magnetic fields and self-heating of thermometers, homemade $SrTiO_3$ capacitors were adopted as thermometers with careful *in situ* calibration [56]. As shown in Fig. 1(e), heat current and the magnetic field are applied along the *ab* plane and the *c* axis of the sample, respectively. Three thermometers measure temperature differences along the *x* ($\Delta T_x = T_1 - T_2$)

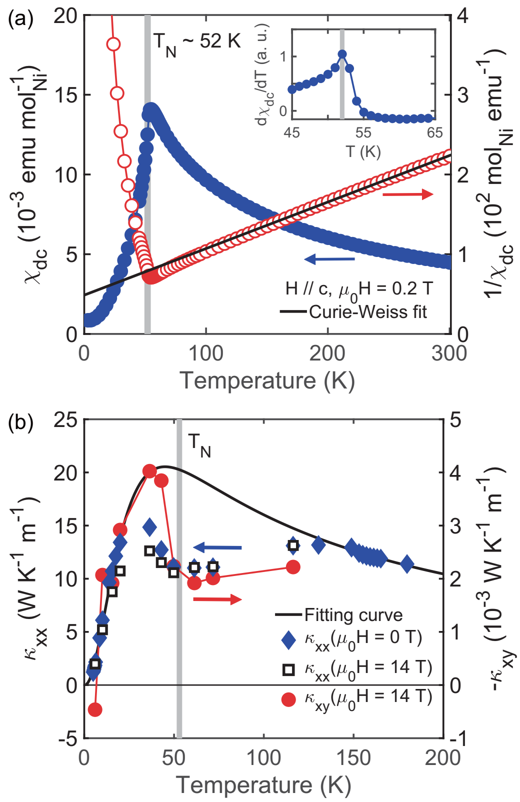

FIG. 2. Measured DC magnetic susceptibility (χ_{dc}) along the c axis, longitudinal thermal conductivity (κ_{xx}), and thermal Hall coefficient (κ_{xy}) as a function of temperature. (a) Blue filled and red open circles display χ_{dc} and $1/\chi_{dc}$, respectively. The inset shows $d\chi_{dc}/dT$ with a clear transition peak near 52 K, indicating an antiferromagnetic phase transition. A solid black line is obtained from the Curie-Weiss law. (b) Blue diamonds and open squares show κ_{xx} at 0 and 14 T, respectively. Red circles show $-\kappa_{xy}$ at a magnetic field of 14 T. The solid black curve is obtained from the Debye-Callaway model by fitting the zero-field κ_{xx} data.

and y ($\Delta T_y = T_3 - T_2$) directions, which can be converted into κ_{xx} and κ_{xy}, respectively [57].

During the sample preparation, contact misalignment between two transverse contacts on the sample (T_2 and T_3) is inevitable. Thus, ΔT_y can contain both true Hall response (δT_y) and a small amount ($|\alpha| \ll 1$) of the longitudinal component ($\alpha\Delta T_x$), i.e., $\Delta T_y = \delta T_y + \alpha\Delta T_x$. Here we should note that $\alpha\Delta T_x$ usually dominates the measured ΔT_y since the typical size of δT_y is about 1000 times smaller than ΔT_x in the insulator. To extract the accurate value of δT_y from ΔT_y, we applied an antisymmetrization procedure of ΔT_y with opposite magnetic field directions using the following relation, $\delta T_y(+H) = \frac{\Delta T_y(+H) - \Delta T_y(-H)}{2}$, since ΔT_x is symmetric [$\Delta T_x(+H) = \Delta T_x(-H)$] and δT_y is antisymmetric [$\delta T_y(+H) = -\delta T_y(-H)$] with the magnetic field.

III. DATA AND ANALYSIS

Figure 2(a) shows the χ_{dc} measured with a magnetic field of 0.2 T parallel to the c axis after zero-field cooling. With decreasing temperature from 300 K, χ_{dc} follows the Curie-Weiss law exhibiting a single peak near 52 K and converges toward zero rapidly as the temperature goes to 0 K. We determined T_N of NTO as 52 K from the sharp peak in $d\chi_{dc}/dT$ [inset of Fig. 2(a)], consistent with the previous report [46]. The straight black line in Fig. 2(a) is obtained from the Curie-Weiss law with fitting range between 150 and 300 K. The experimental $1/\chi_{dc}$ starts to deviate from the fitting below 100 K, indicating short-range correlations for $T_N < T < 100$ K.

Figure 2(b) displays $\kappa_{xx}(\mu_0 H = 0,\ 14\ \mathrm{T})$ and $\kappa_{xy}(\mu_0 H = 14\ \mathrm{T})$ as a function of temperature. For $T < T_N$, $\kappa_{xx}(T)$ follows the typical phonon thermal conductivity with a peak around 30 K [58]. However, $\kappa_{xx}(T)$ starts to increase gradually just above T_N, which does not match with the decreasing nature of typical phonon conductivity at higher temperatures. Interestingly, $\kappa_{xx}(T)$ is restored back to the decreasing behavior for $T > 130$ K, normally expected for phonons. This broad increase of $\kappa_{xx}(T)$ seen for $T_N < T < 130$ K is difficult to understand, especially as there exists strong spin fluctuation in the paramagnetic phase, as found in χ_{dc}. Previous studies found that spin fluctuations would be expected to suppress, not boost, $\kappa_{xx}(T)$ since spin fluctuations can be regarded as an additional scattering source for phonon heat conduction [59–64]. On the other hand, a magnetic field produces negligible effects for $\kappa_{xx}(T)$ for $T > T_N$ whereas there is overall suppression in $\kappa_{xx}(T)$ for $T < T_N$.

As regards thermal Hall measurement, $\kappa_{xy}(T)$ is found to be linearly negative with magnetic fields over the entire temperature range up to twice T_N. For $T > T_N$, finite $\kappa_{xy}(T)$ was observed without further changes even at 120 K. It is well known that magnon Hall conductivity disappears rapidly above a magnetic ordering temperature [21–24]. Therefore, we can assume that $\kappa_{xy}(T)$ in NTO should originate from other sources for $T > T_N$, for which the phonon is a natural candidate. Upon cooling from T_N, the magnitude of $\kappa_{xy}(T)$ increases rapidly with a peak around 30 K before being suppressed at lower temperature. Hence, both $\kappa_{xx}(T)$ and $\kappa_{xy}(T)$ show a very similar temperature dependence in NTO. This similiarity again reinforces our conclusion that the PHE is most likely to be dominant in the AFM phase of NTO, as in Refs. [34–38].

The detailed field dependences of both $\kappa_{xx}(H)$ and $\kappa_{xy}(H)$ are shown in Figs. 3(a) and 3(b), respectively. For $T > T_N$, $\kappa_{xx}(H)/\kappa_{xx}(0)$ increases by less than 1%, which can be interpreted as phonon scattering due to spin fluctuations in the paramagnetic state: The magnetic field aligns the spin moment, and thereby lowers the phonon scattering rate [23,26,27,40,61,65]. On the other hand, the overall decreasing behavior of $\kappa_{xx}(H)/\kappa_{xx}(0)$ seen for $T < T_N$ indicates that the dominant phonon scattering mechanism in the ordered phase is different from those in the paramagnetic phase. As temperature lowers, $\kappa_{xx}(H)$ behaves in a more complex manner, showing an upturn and a sharp suppression in $\kappa_{xx}(H)$ seen around $\mu_0 H \sim 8.5$ T, the critical field (H_c) of the spin-flop transition [46]. This anomaly can be interpreted as an abrupt change of phonon scattering during the magnetic phase transition, adding further evidence for the strong spin-phonon coupling in NTO. On the other hand, $\kappa_{xy}(H)$ shows linear field dependence for all the measured temperatures [Fig. 3(b)]. It

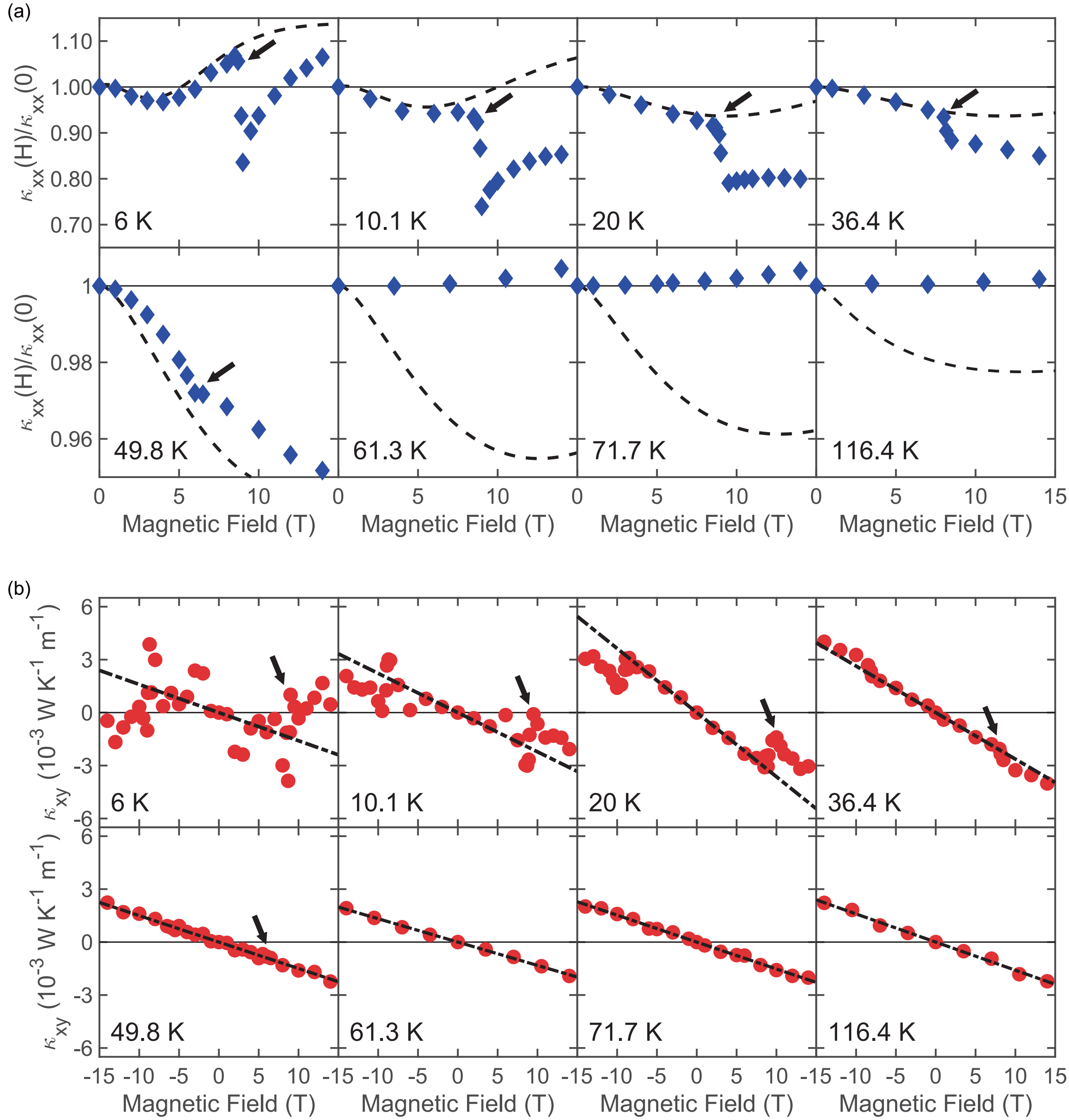

FIG. 3. Measured magnetothermal conductivity [$\kappa_{xx}(H)/\kappa_{xx}(0)$] and thermal Hall coefficient (κ_{xy}) as a function of magnetic field. (a) Blue diamonds show $\kappa_{xx}(H)/\kappa_{xx}(0)$ at various temperature points. Black dashed curves are obtained from the Debye-Callaway model. (b) The red circles show the field dependence of κ_{xy} at various temperatures. Black dash-dotted lines are guides to the eye clarifying the dominant linearity of κ_{xy}, especially in the low-field collinear antiferromagnetic phase. Black arrows indicate a sharp anomaly on κ_{xx} and κ_{xy} due to the spin-flop transition.

is noticeable that at lower temperatures $\kappa_{xy}(H)$ also shows an anomaly at the spin-flop transition, which is similar to $\kappa_{xx}(H)$.

According to the Boltzmann transport equation, phonon thermal conductivity ($\kappa_{xx}^{\mathrm{ph}}$) can be expressed in terms of specific heat (C), group velocity (v), and relaxation time (τ) of the phonon: $\kappa \sim \frac{1}{3}Cv^2\tau$. Since the specific heat shows negligible magnetic field effect in NTO [45], we can conclude that τ should play a more dominant role in the field dependence of $\kappa_{xx}^{\mathrm{ph}}$ by assuming negligible field effect in v. Hence, we adopted the Debye-Callaway model of Eq. (1), a phenomenological model [1], to analyze the field dependence of $\kappa_{xx}(H)$ in the ordered phase of NTO:

$$\kappa_{xx}^{\mathrm{ph}} = \frac{k_B^4}{2\pi^2 v\hbar^3}T^3\int_0^{\frac{T_D}{T}}\frac{x^4e^x}{(e^x-1)^2}\tau(\omega, T)dx, \quad (1)$$

where $\tau^{-1}(\omega, T)$ is the scattering rate of the phonon, T_D is the Debye temperature, ω is the frequency of the phonon, and $x = \frac{\hbar\omega}{k_B T}$ is the phonon energy normalized by the thermal energy. v is estimated from the Debye model using the following relation: $T_D = v\frac{\hbar}{k_B}(6\pi^2 n)^{1/3}$, where n is the number of atoms per unit volume. $\tau^{-1}(\omega, T)$ can then be approximated by a sum of possible scattering sources following Matthiessen's rule: sample boundary (τ_{BD}^{-1}), linear defects (τ_{LD}^{-1}), point defects (τ_{PD}^{-1}), umklapp process (τ_U^{-1}), and resonant phonon scattering process (τ_{res}^{-1}),

$$\tau^{-1}(\omega, T) = \tau_{\mathrm{BD}}^{-1} + \tau_{\mathrm{LD}}^{-1} + \tau_{\mathrm{PD}}^{-1} + \tau_U^{-1} + \tau_{\mathrm{res}}^{-1}. \qquad (2)$$

Each τ_{BD}^{-1} [66], τ_{LD}^{-1} [67], τ_{PD}^{-1} [68], and τ_U^{-1} [58–60] can be modeled as in Eq. (3),

$$\tau^{-1}(\omega, T) = \frac{v}{d} + A_0\omega + A_1\omega^4 + A_2\omega^2 T \exp\left(-\frac{T_D}{bT}\right) + \tau_{\mathrm{res}}^{-1}. \qquad (3)$$

The first four terms in Eq. (3) are enough for obtaining representative phonon thermal conductivity, but these are, *a priori*, assumed to be field independent. For field-dependent κ_{xx}, we thus considered the resonant phonon scattering process (τ_{res}^{-1}) as described in Fig. 4(a). In this scenario, the low-lying magnon bands having a higher density of states (DOS) split linearly under the magnetic field with an energy difference of $\hbar\omega_{\mathrm{res}}$. We note that our hypothesis of the low-lying magnon band with a large DOS is consistent with the recent spin-wave measurement [49]. This process then allows phonons to be scattered by magnons having the specific energy of $\hbar\omega_{\mathrm{res}}$ [58]. We chose an empirical formula for τ_{res}^{-1} of Eq. (4), which has been shown to successfully explain κ_{xx} in several complex magnetic insulators [50–53]:

$$\tau_{\mathrm{res}}^{-1} = R\frac{\omega^4}{(\omega^2 - \omega_{\mathrm{res}}^2)^2}\frac{\exp\left(-\frac{\hbar\omega_{\mathrm{res}}}{k_B T}\right)}{1 + \exp\left(-\frac{\hbar\omega_{\mathrm{res}}}{k_B T}\right)}, \qquad (4)$$

where R indicates the strength of resonant phonon scattering.

Linearly splitting magnon bands shown in Fig. 4(b) could be natural for NTO, since the magnon modes ($\mathcal{E}_\pm$) in the collinear easy-axis AFM phase can be written as Eq. (5) under the magnetic field applied along the easy axis [69]. We further note that our scenario of the resonant phonon scattering process from the magnon makes sense, given that the decreasing $\kappa_{xx}(H)$ happens only below T_{N}. As a result, we can get $\hbar\omega_{\mathrm{res}} = 2g\mu_B\mu_0 H$, where μ_B is the Bohr magneton and $g = 2.26$ is the g factor of NTO [70].

$$\mathcal{E}_\pm(H) = \mathcal{E}(H = 0) \pm g\mu_B\mu_0 H. \qquad (5)$$

Although d, b, T_D, A_0, A_1, A_2, and R in Eqs. (3) and (4) are in principle free parameters, we can put further constraints on several parameters (d, b, and T_D) for a minimum model. First, we can fix d as 1 mm, the shortest in-plane dimension of the sample: d represents the phonon mean free path due to collisions from the sample boundary. Next, b, the characteristic constant of the phonon dispersion, can be fixed using a conventional value of $2\sqrt[3]{N} \sim 6.21$, where N is the number of atoms in a unit cell [59,60,71]. To determine the appropriate value of T_D, we fitted the specific heat data taken from previous studies [48,72]; using the Debye-Einstein model, we

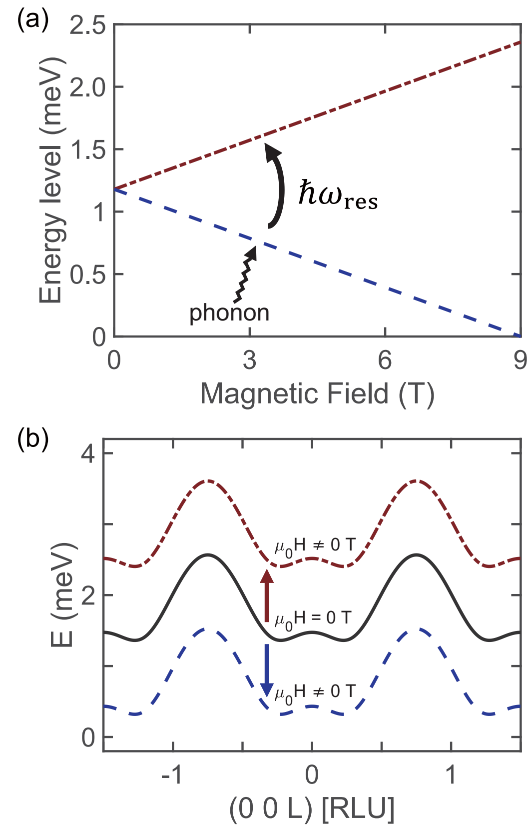

FIG. 4. Schematic of resonant phonon scattering process and effective magnon dispersion of Ni_3TeO_6 in collinear antiferromagnetic phase. (a) Two energy levels in low-lying magnon bands get a linear split under the magnetic field. $\hbar\omega_{\mathrm{res}}$ is the energy difference between lower and upper energy levels of the magnon bands. Blue dashed and red dash-dotted lines represent the lower and upper energy levels, respectively. The following process can describe resonant phonon scattering: A lower energy level absorbs a phonon with the energy of $\hbar\omega_{\mathrm{res}}$, resulting in excitation of the upper level [58]. (b) Effective magnon dispersion in the low-field phase was obtained from Ref. [49]. The black curve shows the dispersion at a zero magnetic field. With a magnetic field, the magnon dispersion starts to split. The red-dotted and blue dashed curves show the dispersion with a finite field.

estimated $T_D = 470$ K. As a result, the free parameters can be reduced to only four A_0, A_1, A_2, and R, all of which indicate the strength of each scattering process.

The fitting result is shown as black dashed curves in Fig. 3(a), and the best fitting parameters are summarized in Table I. The sizes of these values are comparable to previous studies, which also employed the Debye-Callaway model in their analysis [50–53,59]. The calculated $\kappa_{xx}^{\mathrm{ph}}(H)/\kappa_{xx}^{\mathrm{ph}}(0)$ reproduces well the overall behavior of $\kappa_{xx}(H)/\kappa_{xx}(0)$ for $T < T_{\mathrm{N}}$ and $H < H_{\mathrm{c}}$, including the upturn seen for T<10 K. It is not surprising to find, though, that the fitting breaks down for $T \geqslant T_{\mathrm{N}}$ since the magnon will no longer be well defined in the paramagnetic phase. From this exercise, we can conclude that the resonant phonon scattering model may as well be a reasonable explanation for $\kappa_{xx}(H)$ in NTO. However, we admit that our model cannot explain the data in the higher-field region $\kappa_{xx}(H > H_{\mathrm{c}})$. It is mainly due to the fact that the

TABLE I. The best fitting parameters obtained for the Debye-Callaway model with their fitting conditions specified.

Parameter (unit)	Fitting condition	Value
$\boldsymbol{v}$ (m/s)	Fixed	3446
$\boldsymbol{d}$ (mm)		1
$\boldsymbol{T_D}$ (K)		470
$\boldsymbol{b}$ (unitless)		6.21
$\boldsymbol{A}_0$ (unitless)	Free	3.29×10^{-4}
$\boldsymbol{A}_1$ (s^3)		6.44×10^{-43}
$\boldsymbol{A}_2$ (s K^{-1})		4.04×10^{-18}
$\boldsymbol{R}$ (s^{-1})		1.77×10^{8}

magnetic structure and Hamiltonian are as yet unknown in the spin-flopped phase.

Using the same parameters, we also calculated $\kappa_{xx}^{\mathrm{ph}}(T)$ at zero field shown as a black solid curve in Fig. 2(b). We can see that the measured $\kappa_{xx}(T)$ is suppressed from $\kappa_{xx}^{\mathrm{ph}}(T)$ in the temperature range of $T_{\mathrm{N}} < T < 130$ K. As previous thermal transport studies pointed out, paramagnetic spin fluctuations could scatter phonons off, resulting in flatlike $\kappa_{xx}(T)$ [59,62–64]. Thus, we can conclude that the significant spin fluctuation and magnon strongly affect the phonon heat transport in NTO.

IV. DISCUSSION

We would now like to discuss the implications of our κ_{xy}. As there is no good simple model for the PHE yet, we can only make general observations by comparing it with other materials having finite κ_{xy}. First, the mechanism proposed for the PHE in nonmagnetic insulator $SrTiO_3$ is hard to apply to NTO because it requires a substantial dielectric constant ($\varepsilon \sim 10^4$) with structural domain [34,44] or quantum paraelectricity [33], none of which can be valid for NTO. Instead, we conjecture that in the paramagnetic phase, the PHE in NTO originates from the secondary effect of significant spin-phonon coupling [20,65]. We also noticed that the size of $\kappa_{xy}(T)$ rapidly increases just below T_{N} [Fig. 2(b)] and $\kappa_{xy}(H)$ starts to show a humplike behavior at H_c [Fig. 3(b)], all of which indicates that the magnetically ordered phase affects κ_{xy} significantly. Since the similar temperature dependence between $\kappa_{xx}(T)$ and $\kappa_{xy}(T)$ implies that both κ_{xx} and κ_{xy} share the origin and the magnon-phonon scattering model describes κ_{xx} well, we suggest that the magnon-phonon interaction is also a dominant factor for κ_{xy} in the AFM phase.

We also anticipate that the magnon-phonon picture presented here could be used to understand other recent thermal Hall experiments properly. For example, the latest study found that temperature dependences between $\kappa_{xx}(T)$ and $\kappa_{xy}(T)$ in Cu_3TeO_6 are very similar to each other [38], which indicates PHE. We note that Cu_3TeO_6 also shows rapidly increasing $\kappa_{xy}(T)$ for $T < T_{\mathrm{N}}$ [38], similar to NTO. From this, we suggest that magnon-phonon interaction also plays a significant role in Cu_3TeO_6 for $\kappa_{xy}(T)$, which is consistent with the inelastic neutron scattering study [73]. Furthermore, we can find that $\kappa_{xx}(H)$ and $\kappa_{xy}(H)$ of NTO are quite similar to those of $Fe_2Mo_3O_8$, another polar collinear AFM along the c axis accompanying the spin-flip transition [32]. We expect that our model can also be used to explain the data in $Fe_2Mo_3O_8$.

To summarize, we measured both κ_{xx} and κ_{xy} of Ni_3TeO_6. We observed finite negative κ_{xy} up to two times T_{N} and a similar temperature dependence between κ_{xy} and κ_{xx}, which indicates PHE in Ni_3TeO_6. The collinear AFM phase has κ_{xx} well described by the Debye-Callaway model with resonant phonon scattering from the magnon band. We suggest that the same origin governs both κ_{xx} and κ_{xy}: spin-phonon coupling for $T > T_{\mathrm{N}}$ and magnon-phonon interaction for $T < T_{\mathrm{N}}$. We expect that the PHE from the magnon-phonon interaction could be applied to other insulating magnets in the magnetically ordered phase.

ACKNOWLEDGMENTS

We want to thank Ysun Choi for the helpful discussion. The work at SNU was supported by the Leading Researcher Program of Korea's National Research Foundation (Grant No. 2020R1A3B2079375). The work at Rutgers University was supported by the DOE under Grant No. DOE: DE-FG02-07ER46382. J.H.L. and Y.S.O. acknowledge support from the Basic Science Research Programs through the

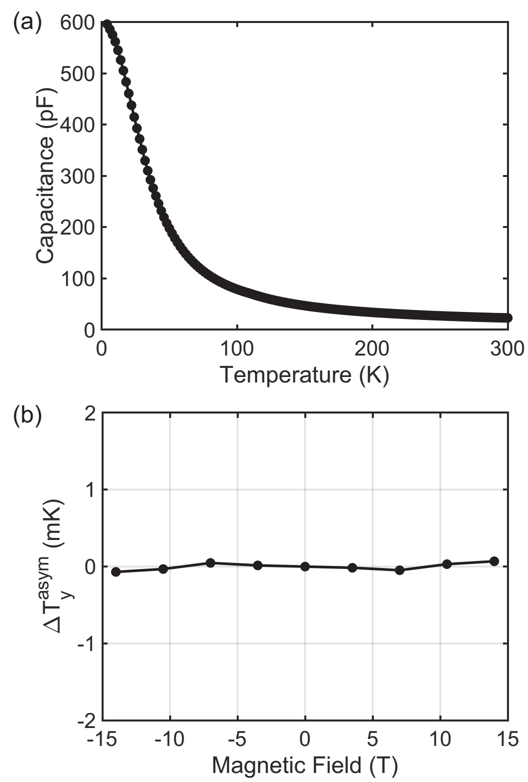

FIG. 5. Typical capacitance value of homemade $SrTiO_3$ capacitive thermometer and result of control experiment. (a) Capacitance of $SrTiO_3$ thermometer is given as a function of temperature down to 4 K: The capacitance grows monotonically as the temperature gets lowered. (b) Antisymmetrized transverse temperature difference ($\Delta T_y^{\mathrm{asym}}$) obtained from control experiment at 20 K, in which we turned off the heat current along the sample.

National Research Foundation of Korea (NRF) (Grant No. NRF-2020R1A2C1009537).

APPENDIX

1. $SrTiO_3$ capacitive thermometry for thermal Hall measurement

Both side-polished $SrTiO_3$ wafers of 0.1 mm thickness were purchased from Crystal GmbH and cut into size of $1 \times 1\,\mathrm{mm}^2$ by a diamond wire saw, to make parallel plate geometry. After evaporation of the 50 nm layer of gold, silver epoxy was coated on both sides. Silver wire of 127 μm diameter was then used to connect the sample and the thermometers to maximize thermal conductance between them. To minimize heat leak through the thermometers, we adopted phosphor bronze wire of 25 μm diameter as leads; this is known to have poor thermal conductance.

Typical temperature dependence of capacitance for the $SrTiO_3$ capacitive thermometer shows monotonic increasing as temperature goes down to 4 K [see Fig. 5(a)]. Before thermal Hall measurement, we always performed *in situ* calibration under the zero magnetic field at each target temperature to further minimize calibration errors. We did not calibrate our thermometer for different magnetic field values since the dielectric constant of $SrTiO_3$ is known to show negligible magnetic field effect [74].

During the thermal Hall measurement, we applied a static magnetic field at each field step and waited around 15 min to eliminate possible error from the magnetocaloric effect. We also conducted a control experiment to check the uncertainty of our measurement setup by measuring antisymmetrized ΔT_y without ΔT_x. As shown in Fig. 5(b), the uncertainty is less then 0.1 mK, which is much smaller than typical Hall response on the order of 1 mK. Further technical information is available in Ref. [56].

2. Fitting procedure for Debye-Callaway model

Before starting the fitting the data, it is good to know how each term in the phonon scattering rate of Eq. (2) manipulates $\kappa_{xx}^{\mathrm{ph}}$. At first, τ_{BD}^{-1} affects $\kappa_{xx}^{\mathrm{ph}}$ in the low-temperature region, since the phonon mean free path should be comparable to the sample size for significant boundary scattering [58]. Next, the presence of τ_{LD}^{-1} and τ_{PD}^{-1} gives overall suppression of $\kappa_{xx}^{\mathrm{ph}}$ for a wide temperature range, and τ_{U}^{-1} tunes the degree of decreasing behavior of $\kappa_{xx}^{\mathrm{ph}}$ for the high-temperature range. Finally, τ_{res}^{-1} mainly gives field dependence to $\kappa_{xx}^{\mathrm{ph}}$ in our model. We assumed all parameters in Eq. (3) and (4) are independent of both temperature and magnetic field.

Considering the above properties of each scattering process, we could roughly determine the initial parameter set for $\kappa_{xx}(T, \mu_0 H = 0\,\mathrm{T})$ without considering τ_{res}^{-1} first. Then, we started to use τ_{res}^{-1} to fit both $\kappa_{xx}(T, \mu_0 H = 0\,\mathrm{T})$ and magnetothermal conductivity $[\kappa_{xx}(H)/\kappa_{xx}(0)]$ simultaneously, by minimizing χ^2. To find the best parameter set shown in Table I, we used the particle swarm optimization algorithm [75], which is powerful for seeking the global mimimum of a complex nonlinear function with broad parameter space.

[1] J. Callaway, Phys. Rev. **113**, 1046 (1959).

[2] C. Kittel, Phys. Rev. **110**, 836 (1958).

[3] J. Oh, M. D. Le, H.-H. Nahm, H. Sim, J. Jeong, T. G. Perring, H. Woo, K. Nakajima, S. Ohira-Kawamura, Z. Yamani, Y. Yoshida, H. Eisaki, S. W. Cheong, A. L. Chernyshev, and J.-G. Park, Nat. Commun. **7**, 13146 (2016).

[4] T. Kim, K. Park, J. C. Leiner, and J.-G. Park, J. Phys. Soc. Jpn. **88**, 081003 (2019).

[5] G. S. Dixon, Phys. Rev. B **21**, 2851 (1980).

[6] G. S. Dixon, V. Benedict, and J. E. Rives, Phys. Rev. B **21**, 2865 (1980).

[7] J. A. H. M. Buys and W. J. M. de Jonge, Phys. Rev. B **25**, 1322 (1982).

[8] X. Zhang, Y. Zhang, S. Okamoto, and D. Xiao, Phys. Rev. Lett. **123**, 167202 (2019).

[9] S. Park and B.-J. Yang, Phys. Rev. B **99**, 174435 (2019).

[10] G. Go, S. K. Kim, and K.-J. Lee, Phys. Rev. Lett. **123**, 237207 (2019).

[11] S. Zhang, G. Go, K.-J. Lee, and S. K. Kim, Phys. Rev. Lett. **124**, 147204 (2020).

[12] H. Katsura, N. Nagaosa, and P. A. Lee, Phys. Rev. Lett. **104**, 066403 (2010).

[13] J. Nasu, J. Yoshitake, and Y. Motome, Phys. Rev. Lett. **119**, 127204 (2017).

[14] R. Matsumoto and S. Murakami, Phys. Rev. Lett. **106**, 197202 (2011).

[15] S. A. Owerre, J. Phys.: Condens. Matter **28**, 386001 (2016).

[16] K.-S. Kim, K. H. Lee, S. B. Chung, and J.-G. Park, Phys. Rev. B **100**, 064412 (2019).

[17] R. R. Neumann, A. Mook, J. Henk, and I. Mertig, Phys. Rev. Lett. **128**, 117201 (2022).

[18] L. Zhang, J. Ren, J.-S. Wang, and B. Li, Phys. Rev. Lett. **105**, 225901 (2010).

[19] T. Qin, J. Zhou, and J. Shi, Phys. Rev. B **86**, 104305 (2012).

[20] C. Strohm, G. L. J. A. Rikken, and P. Wyder, Phys. Rev. Lett. **95**, 155901 (2005).

[21] Y. Onose, T. Ideue, H. Katsura, Y. Shiomi, N. Nagaosa, and Y. Tokura, Science **329**, 297 (2010).

[22] T. Ideue, Y. Onose, H. Katsura, Y. Shiomi, S. Ishiwata, N. Nagaosa, and Y. Tokura, Phys. Rev. B **85**, 134411 (2012).

[23] M. Hirschberger, R. Chisnell, Y. S. Lee, and N. P. Ong, Phys. Rev. Lett. **115**, 106603 (2015).

[24] H. Zhang, C. Xu, C. Carnahan, M. Sretenovic, N. Suri, D. Xiao, and X. Ke, Phys. Rev. Lett. **127**, 247202 (2021).

[25] M. Hirschberger, J. W. Krizan, R. J. Cava, and N. P. Ong, Science **348**, 106 (2015).

[26] D. Watanabe, K. Sugii, M. Shimozawa, Y. Suzuki, T. Yajima, H. Ishikawa, Z. Hiroi, T. Shibauchi, Y. Matsuda, and M. Yamashita, Proc. Natl. Acad. Sci. USA **113**, 8653 (2016).

[27] H. Doki, M. Akazawa, H.-Y. Lee, J. H. Han, K. Sugii, M. Shimozawa, N. Kawashima, M. Oda, H. Yoshida, and M. Yamashita, Phys. Rev. Lett. **121**, 097203 (2018).

[28] M. Yamashita, M. Akazawa, M. Shimozawa, T. Shibauchi, Y. Matsuda, H. Ishikawa, T. Yajima, Z. Hiroi, M. Oda, H. Yoshida,

H.-Y. Lee, J. H. Han, and N. Kawashima, J. Phys.: Condens. Matter **32**, 074001 (2020).
[29] Y. Kasahara, K. Sugii, T. Ohnishi, M. Shimozawa, M. Yamashita, N. Kurita, H. Tanaka, J. Nasu, Y. Motome, T. Shibauchi, and Y. Matsuda, Phys. Rev. Lett. **120**, 217205 (2018).
[30] Y. Kasahara, T. Ohnishi, Y. Mizukami, O. Tanaka, S. Ma, K. Sugii, N. Kurita, H. Tanaka, J. Nasu, Y. Motome, T. Shibauchi, and Y. Matsuda, Nature (London) **559**, 227 (2018).
[31] T. Yokoi, S. Ma, Y. Kasahara, S. Kasahara, T. Shibauchi, N. Kurita, H. Tanaka, J. Nasu, Y. Motome, C. Hickey, S. Trebst, and Y. Matsuda, Science **373**, 568 (2021).
[32] T. Ideue, T. Kurumaji, S. Ishiwata, and Y. Tokura, Nat. Mater. **16**, 797 (2017).
[33] S. Sim, H. Yang, H.-L. Kim, M. J. Coak, M. Itoh, Y. Noda, and J.-G. Park, Phys. Rev. Lett. **126**, 015901 (2021).
[34] X. Li, B. Fauqué, Z. Zhu, and K. Behnia, Phys. Rev. Lett. **124**, 105901 (2020).
[35] G. Grissonnanche, A. Legros, S. Badoux, E. Lefrançois, V. Zatko, M. Lizaire, F. Laliberté, A. Gourgout, J.-S. Zhou, S. Pyon, T. Takayama, H. Takagi, S. Ono, N. Doiron-Leyraud, and L. Taillefer, Nature (London) **571**, 376 (2019).
[36] G. Grissonnanche, S. Thériault, A. Gourgout, M.-E. Boulanger, E. Lefrançois, A. Ataei, F. Laliberté, M. Dion, J.-S. Zhou, S. Pyon, T. Takayama, H. Takagi, N. Doiron-Leyraud, and L. Taillefer, Nat. Phys. **16**, 1108 (2020).
[37] M.-E. Boulanger, G. Grissonnanche, S. Badoux, A. Allaire, É. Lefrançois, A. Legros, A. Gourgout, M. Dion, C. H. Wang, X. H. Chen, R. Liang, W. N. Hardy, D. A. Bonn, and L. Taillefer, Nat. Commun. **11**, 5325 (2020).
[38] L. Chen, M.-E. Boulanger, Z.-C. Wang, F. Tafti, and L. Taillefer, PNAS **119**, e2208016119 (2022).
[39] É. Lefrançois, G. Grissonnanche, J. Baglo, P. Lampen-Kelley, J. Yan, C. Balz, D. Mandrus, S. E. Nagler, S. Kim, Y.-J. Kim, N. Doiron-Leyraud, and L. Taillefer, Phys. Rev. X **12**, 021025 (2022).
[40] M. Akazawa, M. Shimozawa, S. Kittaka, T. Sakakibara, R. Okuma, Z. Hiroi, H.-Y. Lee, N. Kawashima, J. H. Han, and M. Yamashita, Phys. Rev. X **10**, 041059 (2020).
[41] Y. Hirokane, Y. Nii, Y. Tomioka, and Y. Onose, Phys. Rev. B **99**, 134419 (2019).
[42] M. Mori, A. Spencer-Smith, O. P. Sushkov, and S. Maekawa, Phys. Rev. Lett. **113**, 265901 (2014).
[43] T. Saito, K. Misaki, H. Ishizuka, and N. Nagaosa, Phys. Rev. Lett. **123**, 255901 (2019).
[44] J.-Y. Chen, S. A. Kivelson, and X.-Q. Sun, Phys. Rev. Lett. **124**, 167601 (2020).
[45] J. W. Kim, S. Artyukhin, E. D. Mun, M. Jaime, N. Harrison, A. Hansen, J. J. Yang, Y. S. Oh, D. Vanderbilt, V. S. Zapf, and S.-W. Cheong, Phys. Rev. Lett. **115**, 137201 (2015).
[46] Y. S. Oh, S. Artyukhin, J. J. Yang, V. Zapf, J. W. Kim, D. Vanderbilt, and S.-W. Cheong, Nat. Commun. **5**, 3201 (2014).
[47] M. O. Yokosuk, S. Artyukhin, A. Al-Wahish, X. Wang, J. Yang, Z. Li, S.-W. Cheong, D. Vanderbilt, and J. L. Musfeldt, Phys. Rev. B **92**, 144305 (2015).
[48] I. Živković, K. Prša, O. Zaharko, and H. Berger, J. Phys.: Condens. Matter **22**, 056002 (2010).
[49] J. Lass, C. R. Andersen, H. K. Leerberg, S. Birkemose, S. Toth, U. Stuhr, M. Bartkowiak, C. Niedermayer, Z. Lu, R. Toft-Petersen, M. Retuerto, J. O. Birk, and K. Lefmann, Phys. Rev. B **101**, 054415 (2020).
[50] A. V. Sologubenko, K. Giannó, H. R. Ott, U. Ammerahl, and A. Revcolevschi, Phys. Rev. Lett. **84**, 2714 (2000).
[51] R. Hentrich, A. U. B. Wolter, X. Zotos, W. Brenig, D. Nowak, A. Isaeva, T. Doert, A. Banerjee, P. Lampen-Kelley, D. G. Mandrus, S. E. Nagler, J. Sears, Y.-J. Kim, B. Büchner, and C. Hess, Phys. Rev. Lett. **120**, 117204 (2018).
[52] R. Hentrich, X. Hong, M. Gillig, F. Caglieris, M. Čulo, M. Shahrokhvand, U. Zeitler, M. Roslova, A. Isaeva, T. Doert, L. Janssen, M. Vojta, B. Büchner, and C. Hess, Phys. Rev. B **102**, 235155 (2020).
[53] X. Hong, M. Gillig, R. Hentrich, W. Yao, V. Kocsis, A. R. Witte, T. Schreiner, D. Baumann, N. Pérez, A. U. B. Wolter, Y. Li, B. Büchner, and C. Hess, Phys. Rev. B **104**, 144426 (2021).
[54] R. Sankar, G. J. Shu, B. Karunakara Moorthy, R. Jayavel, and F. C. Chou, Dalton Trans. **42**, 10439 (2013).
[55] X. Wang, F.-T. Huang, J. Yang, Y. S. Oh, and S.-W. Cheong, APL Mater. **3**, 076105 (2015).
[56] H.-L. Kim, M. J. Coak, J. C. Baglo, K. Murphy, R. W. Hill, M. Sutherland, M. C. Hatnean, G. Balakrishnan, and J.-G. Park, Rev. Sci. Instrum. **90**, 103904 (2019).
[57] C. Strohm, Ph.D. thesis, University of Konstanz, 2003.
[58] R. Berman, *Thermal Conductions in Solids* (Clarendon Press, Oxford, 1976).
[59] P. A. Sharma, J. S. Ahn, N. Hur, S. Park, S. B. Kim, S. Lee, J.-G. Park, S. Guha, and S.-W. Cheong, Phys. Rev. Lett. **93**, 177202 (2004).
[60] D. Bansal, J. L. Niedziela, A. F. May, A. Said, G. Ehlers, D. L. Abernathy, A. Huq, M. Kirkham, H. Zhou, and O. Delaire, Phys. Rev. B **95**, 054306 (2017).
[61] C. A. Pocs, I. A. Leahy, H. Zheng, G. Cao, E.-S. Choi, S.-H. Do, K.-Y. Choi, B. Normand, and M. Lee, Phys. Rev. Res. **2**, 013059 (2020).
[62] L. D. Casto, A. J. Clune, M. O. Yokosuk, J. L. Musfeldt, T. J. Williams, H. L. Zhuang, M.-W. Lin, K. Xiao, R. G. Hennig, B. C. Sales, J.-Q. Yan, and D. Mandrus, APL Mater. **3**, 041515 (2015).
[63] Y. Liu, M.-G. Han, Y. Lee, M. O. Ogunbunmi, Q. Du, C. Nelson, Z. Hu, E. Stavitski, D. Graf, K. Attenkofer, S. Bobev, L. Ke, Y. Zhu, and C. Petrovic, Adv. Funct. Mater. **32**, 2105111 (2022).
[64] A. Haglund, Ph.D. thesis, University of Tennessee, Knoxville, 2019.
[65] K. Sugii, M. Shimozawa, D. Watanabe, Y. Suzuki, M. Halim, M. Kimata, Y. Matsumoto, S. Nakatsuji, and M. Yamashita, Phys. Rev. Lett. **118**, 145902 (2017).
[66] C. Herring, Phys. Rev. **95**, 954 (1954).
[67] J. M. Ziman, *Electrons and Phonons* (Clarendon Press, Oxford, 1960).
[68] P. G. Klemens, Proc. Phys. Soc., Sect. A **68**, 1113 (1955).
[69] S. M. Rezende, A. Azevedo, and R. L. Rodríguez-Suárez, J. Appl. Phys. **126**, 151101 (2019).
[70] J. Zupan, D. Kolar, and V. Urbanc, Mater. Res. Bull. **6**, 1353 (1971).
[71] G. A. Slack, Solid State Phys. **34**, 1 (1979).

[72] R. Dawar, R. Babu, K. Ananthasivan, and S. Anthonysamy, J. Nucl. Mater. **493**, 219 (2017).

[73] S. Bao, Z. Cai, W. Si, W. Wang, X. Wang, Y. Shangguan, Z. Ma, Z.-Y. Dong, R. Kajimoto, K. Ikeuchi, S.-L. Yu, J. Sun, J.-X. Li, and J. Wen, Phys. Rev. B **101**, 214419 (2020).

[74] C. Tinsman, G. Li, C. Su, T. Asaba, B. Lawson, F. Yu, and L. Li, Appl. Phys. Lett. **108**, 261905 (2016).

[75] J. Kennedy and R. Eberhart, in *Proceedings of ICNN'95—International Conference on Neural Networks* (IEEE, Cham, Switzerland, 1995), Vol. 4, pp. 1942–1948.